

Proliferating cell nuclear antigen loaded onto double-stranded DNA: dynamics, minor groove interactions and functional implications

Ivaylo Ivanov^{1,*}, Brian R. Chapados^{2,3}, J. Andrew McCammon¹ and John A. Tainer^{2,3,*}

¹Department of Chemistry and Biochemistry, Department of Pharmacology, Howard Hughes Medical Institute and Center for Theoretical Biological Physics, University of California—San Diego, 9500 Gilman Drive, La Jolla, CA 92093-0365, USA, ²Department of Molecular Biology and The Skaggs Institute for Chemical Biology, The Scripps Research Institute, 10550 North Torrey Pines Road, MB4, La Jolla, CA 92037, USA and ³Life Sciences Division, Department of Molecular Biology, Lawrence Berkeley National Laboratory, Berkeley, CA 94720, USA

Received July 20, 2006; Revised and Accepted September 26, 2006

ABSTRACT

Proliferating cell nuclear antigen (PCNA) acts as a biologically essential processivity factor that encircles DNA and provides binding sites for polymerase, flap endonuclease-1 (FEN-1) and ligase during DNA replication and repair. We have computationally characterized the interactions of human and *Archaeoglobus fulgidus* PCNA trimer with double-stranded DNA (dsDNA) using multi-nanosecond classical molecular dynamics simulations. The results reveal the interactions of DNA passing through the PCNA trimeric ring including the contacts formed, overall orientation and motion with respect to the sliding clamp. Notably, we observe pronounced tilting of the axis of dsDNA with respect to the PCNA ring plane reflecting interactions between the DNA phosphodiester backbone and positively charged arginine and lysine residues lining the PCNA inner surface. Covariance matrix analysis revealed a pattern of correlated motions within and between the three equivalent subunits involving the PCNA C-terminal region and linker strand associated with partner protein binding sites. Additionally, principal component analysis identified low frequency global PCNA subunit motions suitable for translocation along duplex DNA. The PCNA motions and interactions with the DNA minor groove, identified here computationally, provide an unexpected basis for PCNA to act in the coordinated handoff of intermediates from polymerase to FEN-1 to ligase during DNA replication and repair.

INTRODUCTION

Proliferating cell nuclear antigen (PCNA) serves as a processivity factor (sliding clamp), encircling DNA at sites of replication and repair (1–5). The sliding clamp constitutes a highly symmetric assembly of three identical subunits. Each subunit consists of two domains. The subunits come together to form a remarkable ring-like structure with characteristic pseudo 6-fold symmetry and a central hole large enough to accommodate double-stranded DNA (dsDNA). The PCNA monomers possess a distinctive α/β fold. Each domain forms a wedge shaped structure with two α -helices packed in an antiparallel arrangement against the face of a β -sheet wedge. In total there are 12 α -helices lining the inner surface of the ring impart structural integrity to the protein assembly. Adjacent domains are packed in a head to tail arrangement, which necessitates a long inter-domain linker passing over the central β -sheet. This overall architecture (1,2,4) is remarkably well preserved across bacterial and eukaryotic clamps despite the lack of sequence similarity.

PCNA is known to interact with many components of the cell's replication and signaling machinery (5) and in this context could facilitate exchange of DNA repair enzymes that recognize a common DNA intermediate (6). Since the association of PCNA and DNA is topological in nature, it has not yet been possible to determine a structure of PCNA loaded onto dsDNA by crystallographic means. Therefore, structural knowledge regarding the overall orientation as well as the precise contacts formed between a sliding clamp and the nucleic acid it encircles has been limited. Furthermore, the static PCNA structures determined to date give little information about possible motions of the clamp that may assist in its translocation along DNA. Much of the focus of recent structural work has been on determining interactions between PCNA surface loops and peptides

*To whom correspondence should be addressed. Tel: +1 858 822 0255; Fax: +1 858 534 4974; Email: iivanov@mccammon.ucsd.edu

*Correspondence may also be addressed to John A. Tainer. Tel: +1 858 784 8119; Fax: +1 858 784 2289; Email: jat@scripps.edu

derived from known PCNA binding proteins, such as flap endonuclease-1 (FEN-1), DNA polymerase δ and ϵ and cyclin-dependent protein kinase inhibitor p21(CIP/WAF1) (5–12).

Since no detailed computational modeling studies have been reported for this system, it would be of general interest to examine the overall conformational flexibility of the sliding clamp, the detailed interactions of residues lining the PCNA hole with DNA and the motions of the PCNA ring, which may promote translocation along dsDNA.

To integrate existing structural understanding of PCNA and to help address key questions regarding structural implications for PCNA interactions, we here apply computational analysis to (i) map out the flexible versus rigid regions of PCNA and establish their relationship to known binding motifs; (ii) examine the overall motions of the PCNA ring and (iii) establish if dynamical coupling exists between the three identical subunits and if such coupling could be affected by sequential binding. This paper is divided into three major parts plus Conclusions and Materials and Methods sections.

First, we trace the time evolution of key interactions between dsDNA and basic residues on the inner surface of the sliding clamp and comment on the overall structural characteristics of the DNA–PCNA complex as well as on the observed competition between the equivalent subunits for binding to the nucleic acid phosphodiester backbone. Second, we quantify the motions of the PCNA ring by carrying out covariance matrix analysis, which exposes the existence of long-range correlations concomitant with changes in DNA binding. Third, we present results from principal component analysis that complement the previous observations and provide more rigorous identification of distinct states for the PCNA–DNA complex with implications for PCNA functions.

MATERIALS AND METHODS

Two systems were set up for classical molecular dynamics simulation: (i) *Archaeoglobus fulgidus* PCNA and (ii) human PCNA. The initial structures were taken from the Protein Data Bank (accession nos 1RWZ and 1VYM, respectively). Crystallographic water molecules were removed. A sequence of dsDNA (5'-ACGTTGACTACCGTCTTGA-GGCAGAGTC-3') in the canonical B-form was generated and inserted vertically through the central hole of the PCNA trimer.

The models were completed by adding hydrogen atoms, counterions and solvent [pre-equilibrated TIP3P (13) water molecules] with the XLeap module of the AMBER 7.0 program. Both Cl^- and Na^+ ions were used to neutralize the overall negative charge of the PCNA–DNA complex and mimic physiological conditions with salt concentration of ~ 120 mM. The models were initially minimized for 1000 steps to remove unfavorable contacts, carefully brought to a temperature of 300 K by velocity rescaling and equilibrated for 0.5 ns with the dsDNA atoms kept fixed. The equilibration was then continued for 1.0 ns without the imposition of restraints.

The production runs were carried out for 25.5 ns for system (i) and 24.5 ns for system (ii) in the isothermal-isobaric

ensemble (NPT) with pressure and temperature maintained constant at 1 atm and 300 K, respectively. The long-range electrostatic interactions were treated using the smooth particle mesh Ewald (SPME) algorithm (14). For the non-bonded short-range interactions, we employed a cutoff of 12 Å with a switching function between 10 and 12 Å. Constraining the bond lengths between hydrogen and heavy atoms to their equilibrium values with the SHAKE algorithm (15) eliminated the fastest vibrational motions and thus, permitted an increased integration time step of 2 fs, while maintaining control over the conserved quantities. The r-RESPA multiple time step method (16) was employed with a 2 fs time step for bonded, 2 fs for short-range, non-bonded interactions, and 4 fs for long-range electrostatic interactions.

The simulation system (i) contained 156 293 atoms in total whereas the simulation system (ii) had 125 056 atoms. All simulations were performed with the program NAMD 2.5 (17) using the AMBER parm99 forcefield parameters (18) on 160 processors of the IBM DataStar system at the San Diego Supercomputing Center.

RESULTS AND DISCUSSION

PCNA interactions with DNA

To examine in detail the relation between existing PCNA structures and their biologically critical functional interactions with dsDNA, we carried out extensive molecular dynamics simulations. The simulation of hPCNA in complex with dsDNA reveals an unexpected and striking tilt of the PCNA ring relative to the DNA axis, as shown by a snapshot taken from the end of the simulation trajectory for the hPCNA/dsDNA system (Figure 1). Furthermore, human PCNA is evidently prototypical for PCNA in general, as analogous results are obtained for archaeal PCNA. The most prominent feature of the structure resulting from the simulation is the pronounced tilt (of $\sim 20^\circ$) in the axis of dsDNA with respect to the plane of the PCNA ring. The right-hand view of the structure shows that the dsDNA helix substantially departs from its initial position at the center of the sliding clamp to form contacts with basic protein residues (arginine and lysine) lining the inner surface of the hPCNA ring. Thus, the helix is no longer symmetrically oriented with respect to hPCNA. Analogous observations are equally valid for *A. fulgidus* PCNA, where the tilt angle approaches 20° towards the end of the simulation.

The observed changes in orientation of the DNA helix with respect to PCNA stem from two major intrinsic structural factors. First, the relatively rigid structure of the sliding clamp preserves the diameter of the central hole of PCNA (~ 35 Å), which is significantly larger than the lateral extent of the dsDNA helix in the canonical B-form (19) (~ 24 Å). Second, the need to maximize the interactions between the positively charged protein residues located on the inner surface α -helices of PCNA and the negatively charged DNA phosphodiester backbone leads to an energetically more favorable tilted orientation for PCNA on dsDNA, as displayed in Figure 2 for hPCNA. The red surface, representing charged residues within a 6 Å cutoff from the DNA phosphate groups, tracks along part of the DNA backbone on both strands of the DNA minor groove and is almost

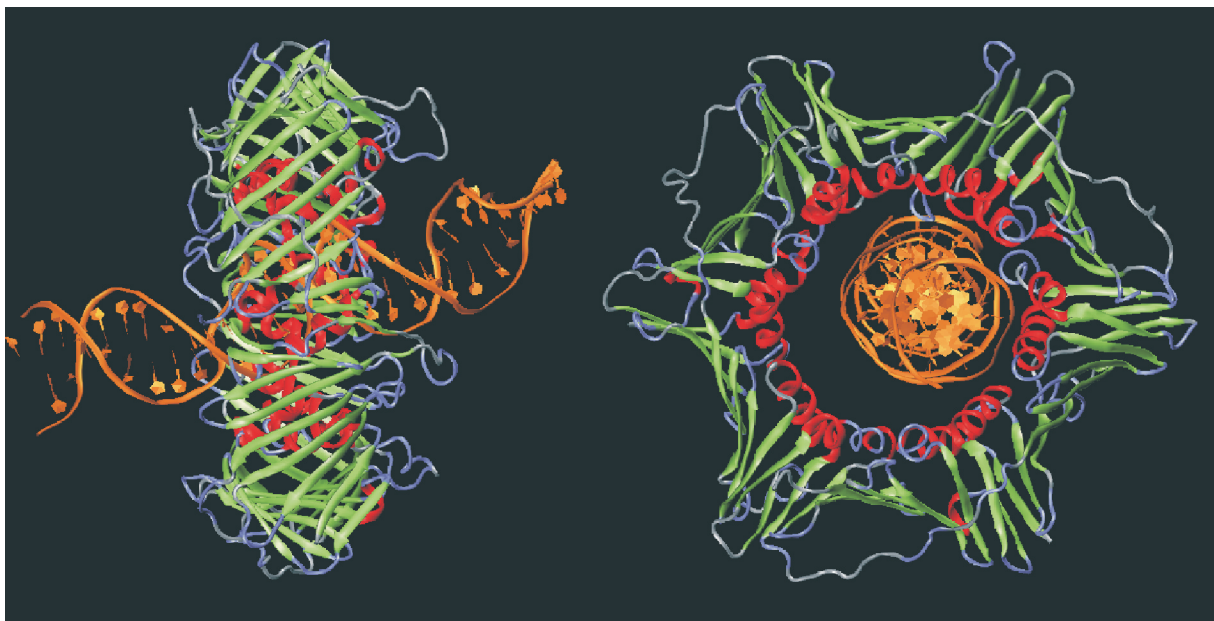


Figure 1. hPCNA top and side view of the final configuration from molecular dynamics. Color-coding scheme according to secondary structure.

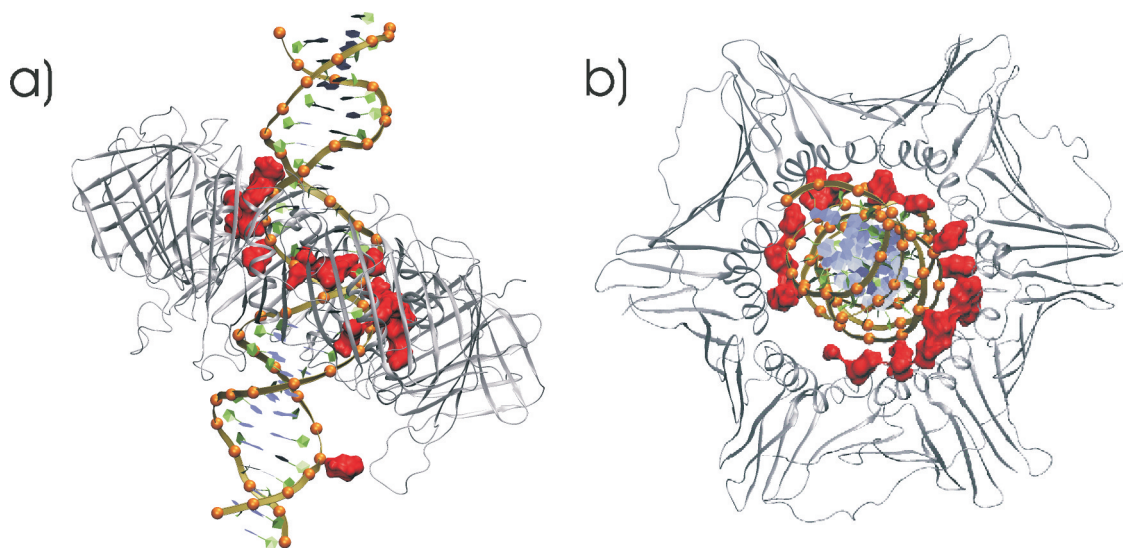


Figure 2. PCNA interactions with dsDNA: a) side view and b) upper view of the hPCNA dsDNA complex reveal the relationship between the tilting of the hPCNA ring with respect to dsDNA and the interactions between the nucleic acid backbone and the inner positively charged surface of the sliding clamp. The dsDNA phosphodiester groups (orange spheres) plus basic (arginine and lysine) groups of hPCNA within 6 Å of the phosphates (red surfaces) are shown.

exactly perpendicular to the axes of the α -helices forming the inner surface of hPCNA (Figure 2). It has been suggested that association perpendicular to the minor groove, as opposed to binding parallel to the major or minor groove seen in many DNA binding proteins, promotes the formation of non-specific protein–DNA interactions and prevents significant distortions in the structure of the nucleic acid (4). Furthermore, the inner diameter of the PCNA ring is large enough to allow the solvent to pass through freely (as observed in the simulations) and compete with the protein residues in making contacts with DNA. Thus, we find that the process of contact breaking and formation along the

inner surface of PCNA is very dynamic, with competition between different protein residues for the phosphodiester groups of DNA.

To analyze the dynamics of contact formation in our simulations, we calculated along the entire trajectory the number of nitrogen atoms belonging to the side chains of positively charged protein residues that were located within 7 Å of a DNA phosphate group. It is informative to examine the distribution of such contacts as a function of the distance between the phosphorus and nitrogen atoms (Figure 3). The histogram data are bimodal and allow us to distinguish between close interactions with P–N distances varying from

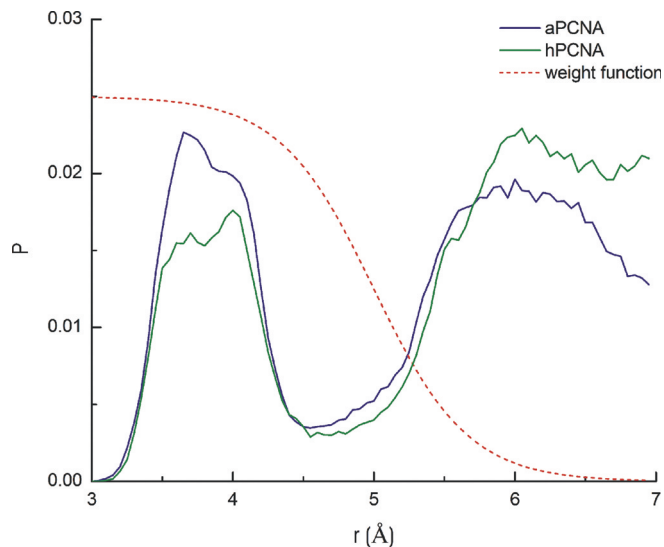


Figure 3. Histogram of the interactions between the side chain N atoms of basic (arginine and lysine) groups of PCNA located within 7 Å of the nucleic acid backbone P atoms. The distribution of nitrogen–phosphorus contacts as a function of distance reveals two peaks with a minimum at ~ 4.6 Å. Thus, the N–P contacts can be naturally subdivided into close (below the minimum) and distant (above the minimum) interactions. This is true for both aPCNA (blue) and hPCNA (green). The red curve represents the weighting function that was used to select ‘close’ interactions. It varies between 0 and 1 and for clarity is not shown to scale.

3.2 to 4.6 Å and more distant interactions above 5 Å. Although weaker than the ‘close’ interactions, the ‘distant’ interactions are nevertheless expected to contribute to the electrostatic stabilization of DNA inside the PCNA central hole due to their larger number and the long-range nature of the Coulomb effect. Figure 4a and b depicts the time evolution of the number of contacts during our simulations.

Besides the total number of contacts found within a 7 Å cutoff, we also calculated a more complicated function, reflecting the larger contribution of ‘close’ interactions. This was accomplished by weighting the number of P–N contacts by a Fermi-like function $f(r) = 1/\{\exp[k(r - r_c)] + 1\}$. The values of r_c and k^{-1} were selected to be 5 Å and 0.333 so that contacts below the minimum in the distributions (at ~ 4.6 Å) are fully weighted whereas contacts above 6 Å have negligible contribution. In determining the number of contacts we take into account the fact that a phosphate group can certainly interact with more than one charged amino acid side chain within the cutoff and vice versa. Therefore, we count the total number of such pairs. For both systems, we observe an overall increase in the number of contacts, which is paralleled closely by an increase in the tilt angle Φ between the axis of the DNA helix and a vector normal to the plane of the PCNA ring (Figure 4c and d).

The results indicate that the number of ‘close’ interactions varies between 5 and 20, and these strong contacts are broken and reformed on a sub-nanosecond timescale (Figure 4). Visual inspection of the trajectory for the hPCNA system revealed that the tilting of the PCNA ring is a relatively simple, gradual transition. In contrast, in the case of aPCNA, we observe initial gradual motion with several excursions back and forth followed by a transition into a more stable tilted

orientation at ~ 7 ns; then the ring of PCNA straightens out and moves with respect to DNA before transitioning into another tilted conformation for the protein nucleic acid assembly. This conformation remains stable until the end of the simulation. The time scale of our simulations is insufficient to sample exhaustively the global motions of clamp with respect to DNA or the process of ‘sliding’ along DNA. However, the results are stunningly suggestive as to why the clamp is capable of ‘sliding freely’ despite the fact that it forms extensive contacts with the nucleic acid backbone. The answer lies in the competition between charged residues on the inner surface of PCNA for forming interaction with the two strands of DNA along a stretch of the minor groove coupled to the ability of the ring to tilt and partially rotate around DNA. This competition is illustrated on Figure 5, which presents the share of P–N contacts with the DNA phosphodiester groups made by each of the PCNA subunits. The numbers vary substantially between the subunits and during the different stages of the simulations. Often an increase in the number of contacts made by one subunit is compensated by a decrease in the interactions with the other two subunits. Notably, this seems to be the case for both hPCNA and aPCNA. We also note that for aPCNA the observed overall increase in the total number of close contacts arises primarily from closer association with dsDNA and subunit C in the latter half of the simulation.

Flexibility of PCNA: B-factors and covariance matrices. Long-range correlations

We examined the covariance and cross-correlation (normalized covariance) matrices for the atoms in our PCNA system with dsDNA (20,21). The covariance matrix elements can be expressed as:

$$c_{ij} = \langle (r_i - \langle r_i \rangle) \cdot (r_j - \langle r_j \rangle) \rangle = \langle r_i \cdot r_j \rangle - \langle r_i \rangle \langle r_j \rangle$$

$$= \frac{\Delta t}{t_{\text{ave}}} \left(\sum_{t=0}^{t_{\text{ave}} - \Delta t} r_i(t) \cdot r_j(t) \right) - \frac{\Delta t}{t_{\text{ave}}} \left(\sum_{t=0}^{t_{\text{ave}} - \Delta t} r_i(t) \right) \times \left(\sum_{t=0}^{t_{\text{ave}} - \Delta t} r_j(t) \right),$$

where t_{ave} is the averaging time, Δt is the time step, the positions atoms i and j at time t are $r_i(t)$ and $r_j(t)$, respectively, and the angular brackets denote time averaging. The diagonal elements of the covariance matrix correspond to the atomic mean square fluctuations and are, in turn, related to the computed isotropic temperature factors (B-factors) by a constant multiplicative factor $8\pi^2/3$. The elements of the cross-correlation matrix are defined as:

$$c_{ij} = \frac{c_{ij}}{c_{ii}^{1/2} c_{jj}^{1/2}}.$$

These take values from -1 to 1 and, in contrast to the covariance coefficients, do not contain information about the magnitude of the correlated motions.

The computed and experimental B-factors on the C α atoms for our systems both serve as a measure of the inherent flexibility of the protein residues within a particular stretch of sequence (Figure 6). The overall agreement between

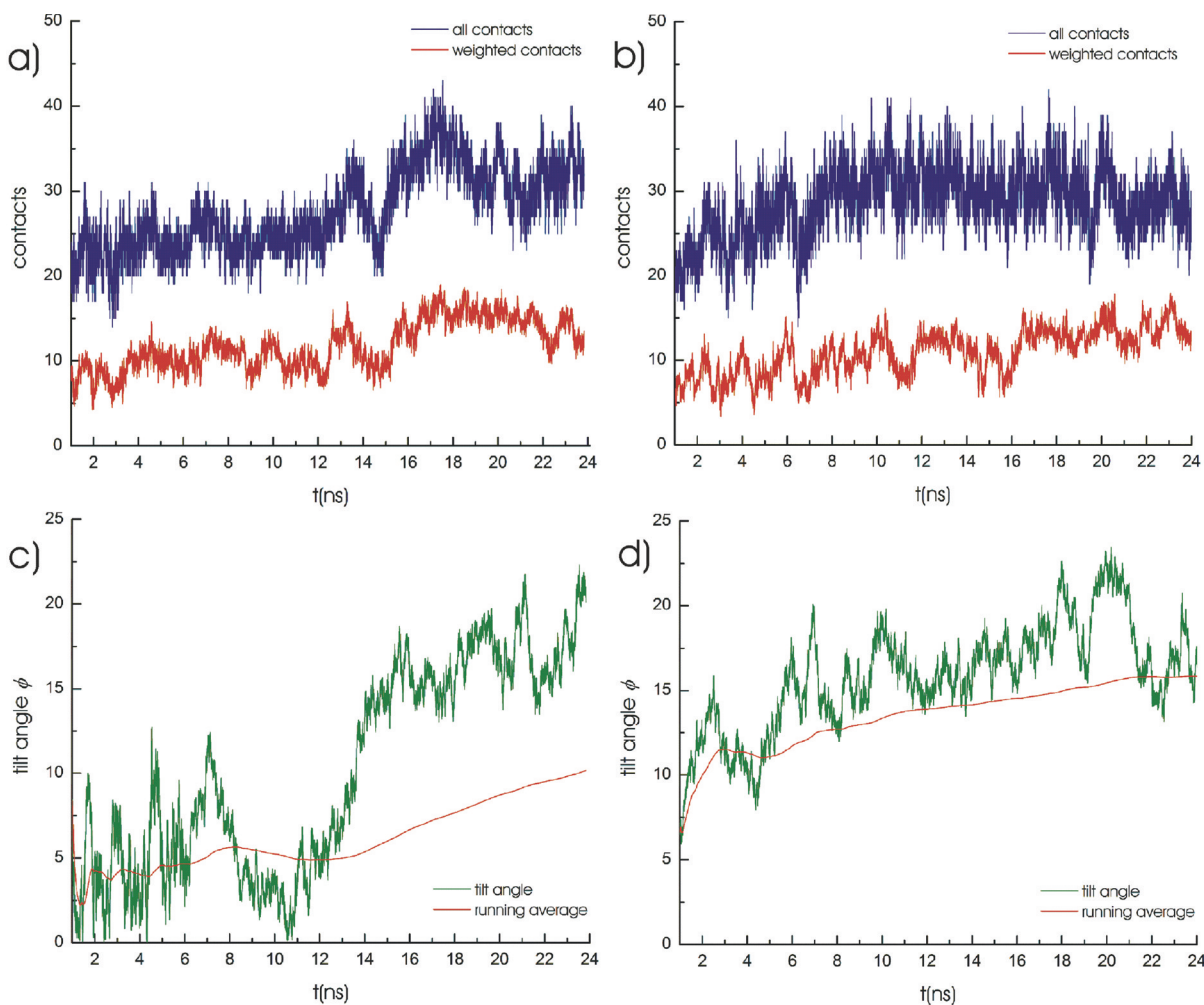


Figure 4. Time evolution of the interactions between the side chain N atoms of basic (arginine and lysine) groups of hPCNA located within 7 Å of the nucleic acid backbone P atoms. Data for aPCNA is shown on (a) and for hPCNA on (b). (c and d) display the time evolution of the tilt angle between the DNA axis and the plane of the PCNA ring for aPCNA and hPCNA, respectively. The observed increase in the number of N–P contacts over the trajectory is closely paralleled by an increase in the tilt angle, which approaches 20° toward the end of the simulations.

theory and experiment is reasonable especially in the case of hPCNA with both experimental and computed B-factors identifying the same mobile regions. That said, the computed B-factors produce sharper peaks and the differences become particularly pronounced at both ends of the sequence. Such differences are not surprising, given that the simulations are supposed to reflect a situation closer to solution phase dynamics whereas the experiment is done under different conditions and on a vastly different timescale.

The calculated covariance and cross-correlation matrices between the C α atoms for both hPCNA and aPCNA reveal a clear pattern of correlated and anticorrelated motions extending both within and between the PCNA subunits (Figure 7). These motions are represented by off diagonal peaks, indicating correlation and valleys, indicating anti-correlation. In general, values in the range above 0.25 and below -0.25 in the cross-correlation matrices can be considered significant. The fact that strong coupling between the motions of the subunits exists opens up the possibility that affecting the dynamics of PCNA in one of the subunits (e.g. through binding) may have consequences for the

dynamics of the other two subunits. On the other hand, such correlation may simply reflect the relatively rigid structure of the clamp and the tight coupling between the individual subunits. Future work is needed to address this issue possibly by carrying out simulations of peptides bound to PCNA.

A key aspect of the cross-correlation maps is that they reveal a non-equivalence of the three PCNA subunits in terms dynamics, with such differences arising from dsDNA binding. The disparity in size between the inner diameter of PCNA and the lateral extent of dsDNA makes it impossible to form equally extensive contacts with all three subunits. For instance, the DNA minor groove associates primarily with subunits A and B of human PCNA, leaving subunit C as the most mobile of the three hPCNA monomers. This is clearly represented in the covariance map (Figure 7a and b), showing the largest covariance values to be associated with subunit C and extensive cross-correlation terms extending into subunit B. For aPCNA the second subunit (chain B in our model structure) displays a pattern of correlation and anticorrelation distinct from the patterns of the other two

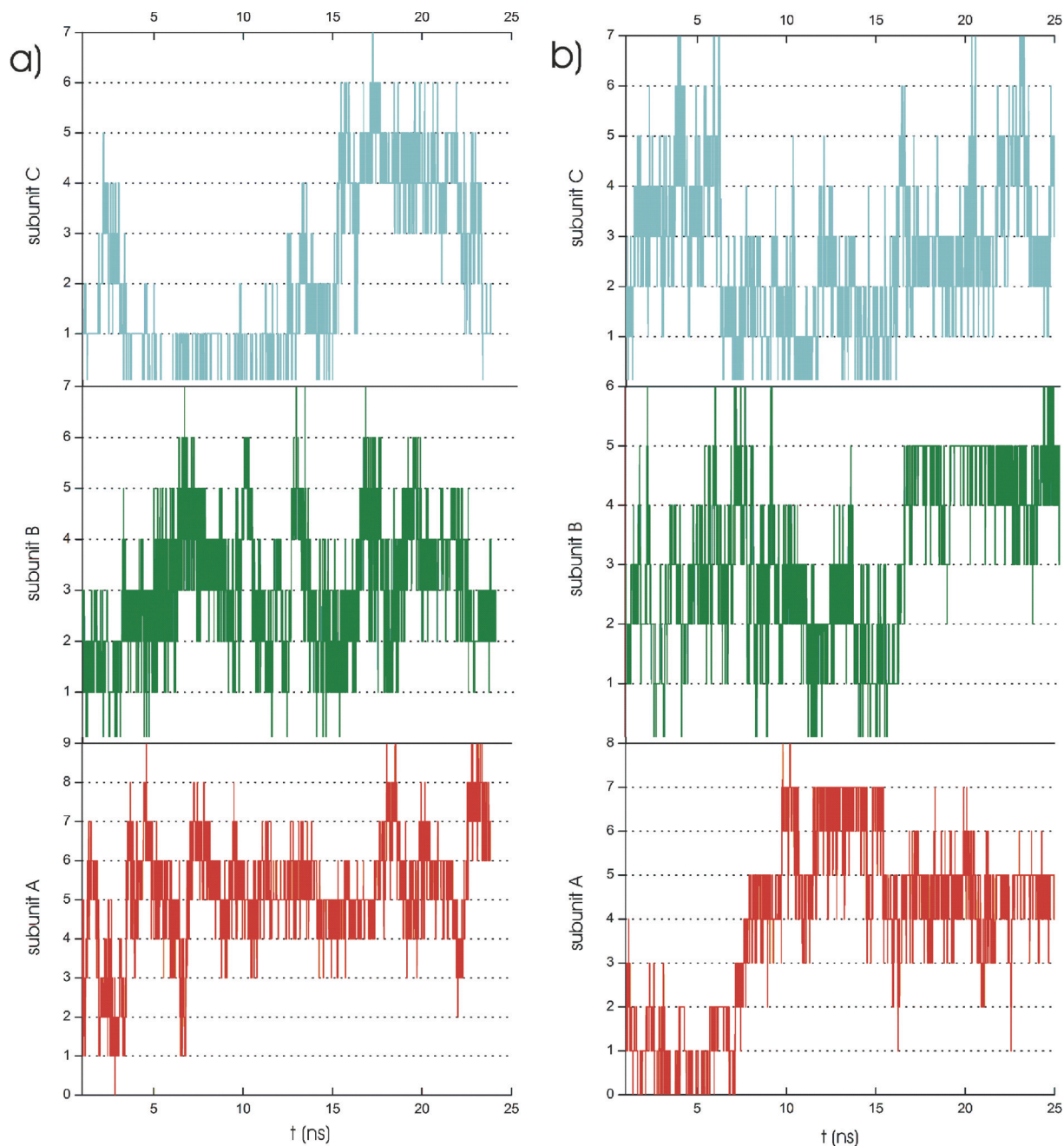


Figure 5. Time evolution of ‘close’ nitrogen–phosphorus contacts (within a 4.6 Å cutoff) between each of the PCNA subunits and the nucleic acid. Data for aPCNA is shown on (a) and for hPCNA on (b), respectively. Individual subunit graphs are highlighted in red, green and blue. The figure essentially represents the share of P–N contacts with the DNA phosphodiester backbone made by each of the PCNA subunits during the simulation, highlighting the dynamic nature of the observed asymmetric binding between the PCNA subunits and DNA.

subunits, which appear to be similar and symmetrically related. The second subunit also exhibits motions of greater magnitude compared to the other two, especially in a region at the PCNA C-terminus (residues 240–244 of the PCNA monomer). These results are potentially informative as the aPCNA C-terminus is known to form part of a hydrophobic pocket on the surface of PCNA responsible for association with PCNA binding enzymes, such as FEN-1 (6). Examination of the trajectory immediately reveals that the B subunit directly associates with the minor groove of dsDNA making

contacts with the phosphodiester backbone throughout the latter part of the simulation. Comparison to Figure 5 shows that the subunit also displays the largest variation in the number of contacts formed during the trajectory confirming its increased mobility. Although the limited length of our simulations precludes a more definitive computational test of contacts and mobility at this time, the results are completely consistent with the proposal that closer association of dsDNA to a given subunit can influence dynamics on the outer surface of the clamp.

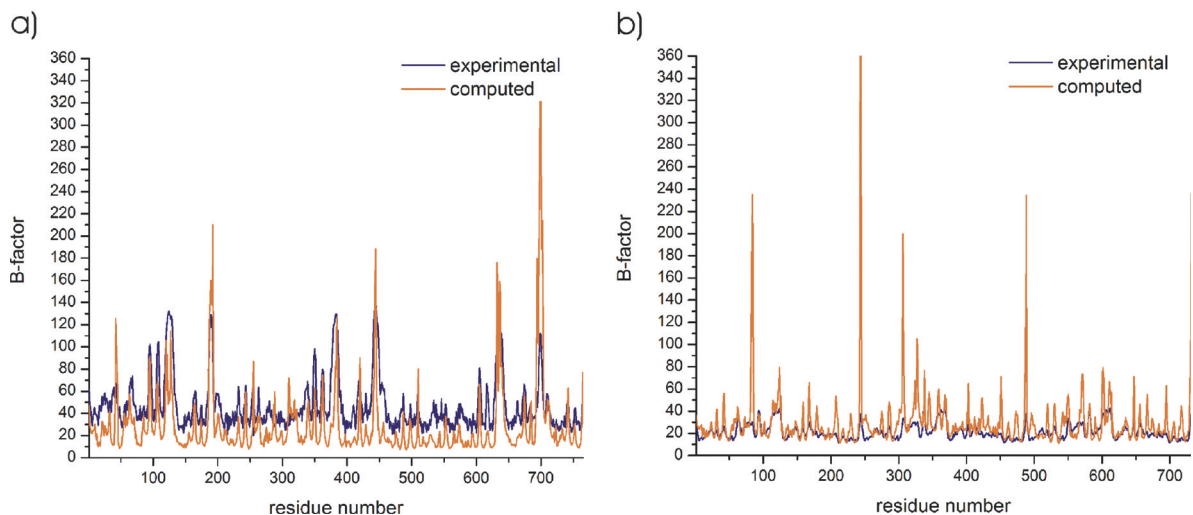


Figure 6. Computed versus experimental B-factors identifying the mobile regions of the PCNA trimer as a function of residue number (with subunits A, B and C shown sequentially): (a) for hPCNA and (b) for aPCNA.

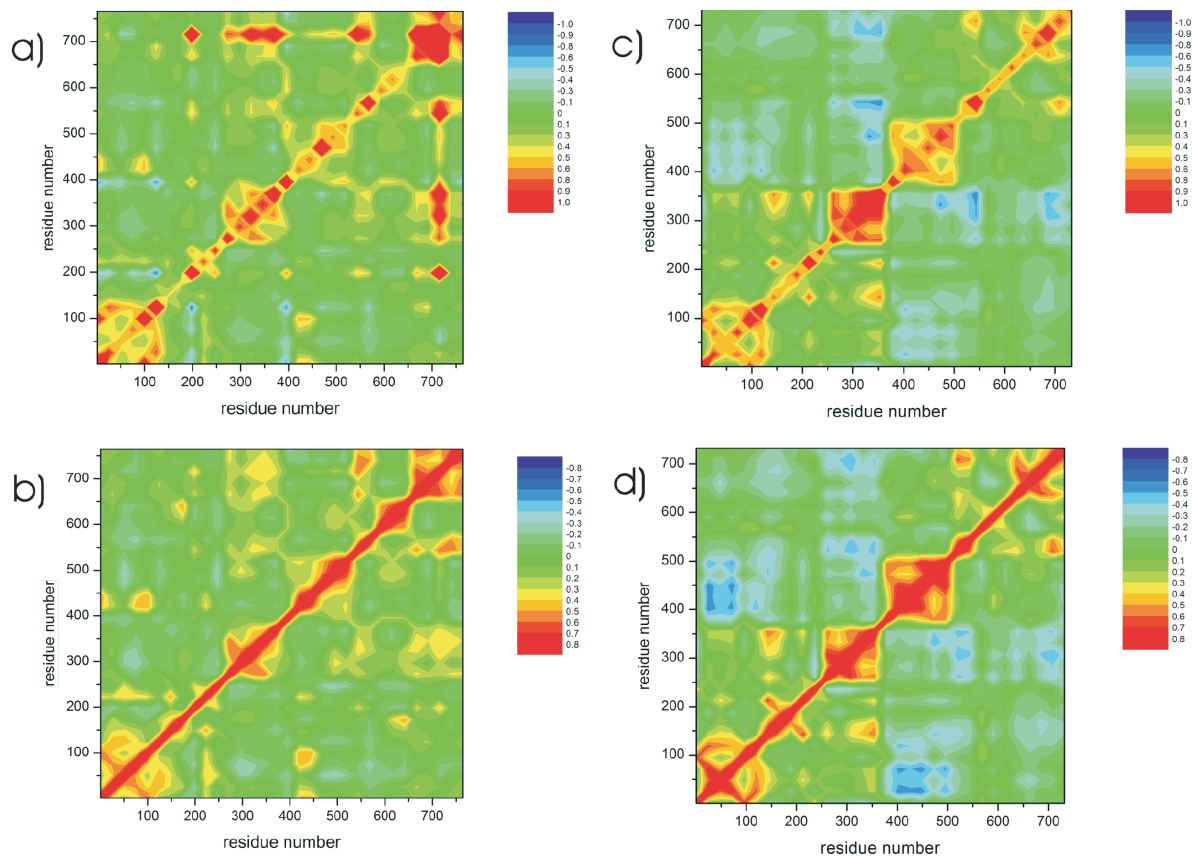


Figure 7. Correlated and anti-correlated PCNA motions revealed by cross-correlation and covariance maps for hPCNA and aPCNA. a) Covariance (a) and cross-correlation matrix (b) for hPCNA; b) Covariance (c) and cross-correlation matrix (d) for aPCNA. The cross-correlation and covariance maps identify regions of the protein that may be distant in the sequence but, nevertheless, move in a concerted way. Positive values (red) denote correlated motions; negative values (blue) indicated anti-correlated motions.

Global collective motions of PCNA on DNA: principal component analysis

To identify and visualize correlated motions, including global collective motions of PCNA on DNA with potential

functional significance, we employed principal component analysis (22–24) (PCA) on both the hPCNA and aPCNA systems. PCA uses the covariance matrix of the C α atoms expressed in Cartesian coordinates. The matrix is symmetric and can be diagonalized using an orthonormal transformation

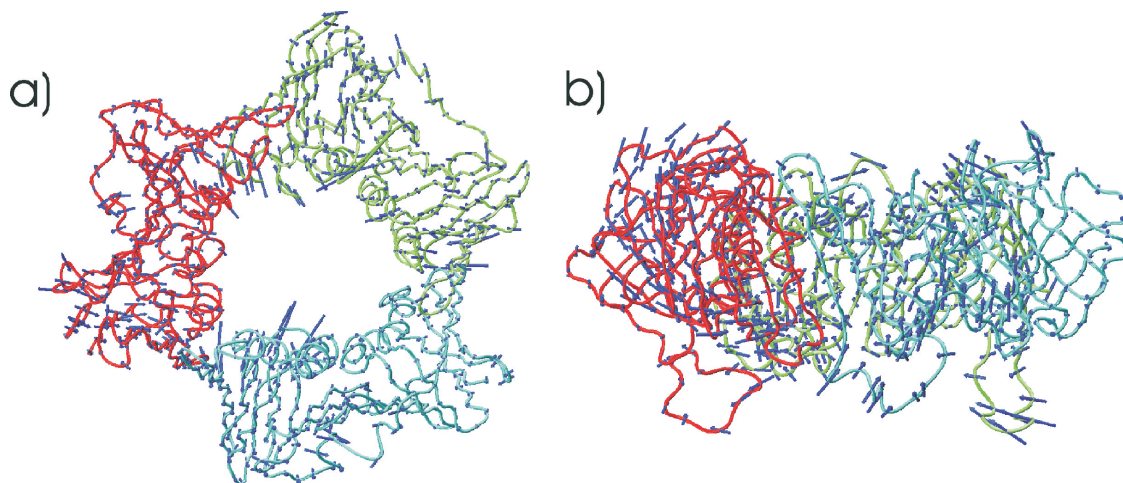


Figure 8. Front (a) and side (b) representations of the first principal component vector mapped onto the C α carbon atoms of hPCNA. The three subunits are shown in trace representation along the C α carbon atoms in red, green and blue, respectively.

matrix R , with eigenvectors denoted as principal modes. Projections of the trajectory onto the principal modes are called the principal components. The eigenvalue corresponding to a principal component represents the mean square fluctuation along this component. We applied a least squares fitting procedure to the average protein structure from the second half of the simulation to eliminate the overall rotational and translational motion of PCNA.

We found PCA to be a versatile tool for analyzing protein dynamics for these systems and useful in confirming observations made during visual inspection of the trajectories. As PCA reduces the dimensionality of the trajectory data, it highlights important dynamical features with the first few principal modes describing collective, global motions of the system. For the two PCNA systems, these involved both the C-terminal region of the PCNA subunits and the central part of the linker strand connecting the two domains of the PCNA molecule. Significantly, these structural elements on the surface of the sliding clamp are largely responsible for binding to DNA-editing enzymes. For example, the first principal component eigenvector mapped onto the C α carbon atoms of hPCNA reveals that the largest motions involve the linker domain and the three flexible loops (guides) of hPCNA (Figure 8). However, we also observe collective rocking/twisting movement of the PCNA domains. This eigenvector accounts for 32% of the overall motion seen in the hPCNA dynamics trajectory. (For comparison, the first five eigenvectors of the covariance matrix are responsible for $\sim 50\%$ of the observed motion because the corresponding eigenvalues decrease rapidly). The magnitude of these motions appears to be largest toward the tips of the wedge shaped domains, but due to the rigid structure of the clamp, the motion also gets propagated to the inner surface alpha helices that make contact with DNA. Such collective motions are interesting in that they appear appropriate to facilitate the translocation of PCNA along dsDNA.

Figure 9 depicts two-dimensional projections of the trajectories for the two systems onto the first and second principal components. The analysis was again carried out using the C α carbon atoms of the protein residues and, therefore, reflects

the interactions with dsDNA only indirectly. Nevertheless, it is interesting to observe several clusters of states along the trajectory especially pronounced in the aPCNA case. As noted above, the hPCNA system seems to undergo a more gradual transition and this fact is reflected on Figure 9a, which shows a smooth transition between two broad basins encompassing many microstates. In contrast, the aPCNA system displays three well-defined basins. The first basin is rather broad reflecting the exploration of conformational space occurring during the initial stage of the simulation. The other two basins are much more compact and are especially pronounced in terms of density. The region between these basins is shallow and possibly serves as an intermediate state in the structural transition described earlier. Thus, the global motions of the sliding clamp with respect to dsDNA appear to be well correlated to the internal motions within the PCNA ring.

General implications

As more structures are determined the value of computational analyses that help clarify their functional interactions becomes increasingly important, especially for the reversible associations linked with many of the major decision points for cells, i.e. cell growth versus death and DNA replication versus repair in the face of damage. PCNA is a recognized master key for reversible associations that determine pathways since it interacts with many replication and repair proteins as well as cell cycle checkpoint inhibitors. For this reason, it has been suggested that PCNA may coordinate its protein partner activities either by forming ternary complexes with two or three replication factors or by handing off DNA intermediates from one enzyme to the next in the replication or repair pathway (5,25–27).

Both mechanisms are based on current models for PCNA encircling DNA, which imply that PCNA is perpendicular to the axis of DNA. In this orientation, the three binding sites, each located on the face of one subunit of the PCNA homotrimer, appear to be equivalent. In contrast, our simulations show that PCNA binds to DNA asymmetrically, mainly

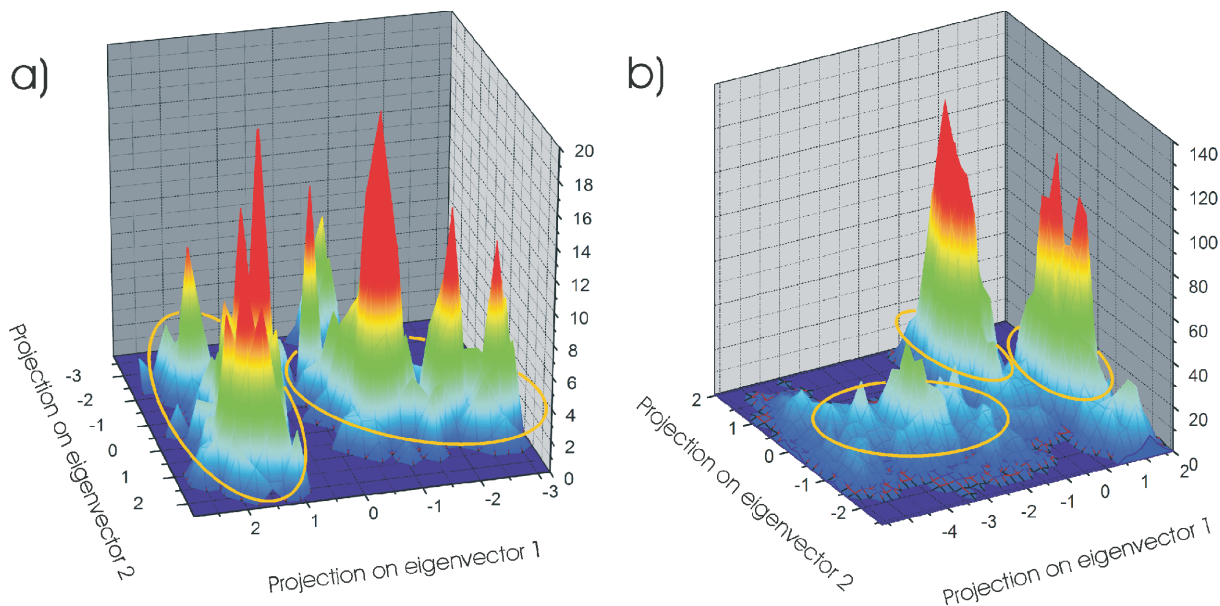


Figure 9. Histograms obtained from two-dimensional projections of the trajectories onto the first two principal eigenvectors. Data for hPCNA and aPCNA is shown in (a) and (b), respectively.

through positively charged residues on the alpha helices that line the inside of the PCNA ring. These residues interact with the phosphate backbone along the minor groove of DNA. This binding mode causes the plane of the PCNA ring to tilt by $\sim 20^\circ$ with respect to the helical axis of DNA, breaking the symmetry of the PCNA trimer. This result has broad implications for the mechanism in which PCNA interacts uniquely with multiple enzymes.

Most efforts to characterize PCNA interactions with replication and repair enzymes have focused on regions of the trimer surface identified by structural analyses of peptides and enzymes bound to PCNA (5,26). Although, it is widely recognized that interactions between PCNA and DNA can influence the nature of PCNA interactions with bound enzymes, these interactions are difficult to characterize using biophysical techniques. For example, PCNA stimulates the activity of enzymes, such as DNA pol δ and FEN-1, but only when PCNA encircles DNA (25,28,29). Structural and biochemical studies suggest that residues from FEN-1 and the C-terminus of PCNA form a β -sheet, which positions FEN-1 for catalysis (6,29). Notably, our simulations indicate that the loop and C-terminal regions of each PCNA subunit, which are involved in partner enzyme interactions, may exhibit differences in flexibility depending on their association with DNA. Such changes in flexibility appear suitable to aid handoffs between different enzymes or facilitate unique interactions with simultaneously bound enzymes based on contacts between PCNA and DNA.

Previous experimental evidence highlights the importance of specific interactions between PCNA and DNA. Our simulation results identified several positively charged Arg and Lys residues that potentially interact with the phosphate backbone of DNA (Figure 2): Lys13, Lys14, Lys20, Lys77, Lys217, Arg146 and Arg149. All of these residues are located on the inner surface of the PCNA ring and are conserved in both human and yeast PCNA. Previous mutational analyses

showed that mutating Lys20 or Lys77 to Glu interfered with mismatch repair in *Saccharomyces cerevisiae*, resulting in a mutator phenotype (30). Biochemical analyses using purified human PCNA and pol δ showed that mutating these PCNA residues to Ala prevented PCNA from stimulating pol δ polymerization, but did not affect the processivity of the pol δ :PCNA complex (31). These PCNA mutants were originally thought to interfere with initiation of DNA synthesis by pol δ (31). Importantly, our results support this interpretation and suggest that the tilted orientation of PCNA relative to the helical axis of DNA, facilitated by charged interactions with the DNA backbone, could uniquely position pol δ for efficient initiation of DNA synthesis.

If the asymmetric orientation of PCNA is critical for stimulating pol δ initiation, then this orientation might also be required to stimulate FEN-1 activity (6,32,33). This hypothesis can now be experimentally tested using an established biochemical assay for measuring the activity of FEN-1 in the presence of PCNA that has been loaded onto DNA by RFC (29). Mutations of the basic amino acids lining the center of the PCNA do not affect RFC-dependent loading or activity (31). Thus, these mutations, which disrupt interactions with DNA backbone along the minor groove, could be used to test whether the asymmetric orientation of PCNA is required to stimulate FEN-1 activity. In addition, several key charged residues are also conserved in the heterotrimeric PCNA homolog from *Sulfolobus solfataricus* (34). In this organism, FEN-1 and DNA polymerase each bind to a single subunit of the heterotrimer. Thus, mutational analysis in this PCNA homolog could be used to determine how DNA interactions with a single subunit affect interactions with a bound enzyme.

The DNA binding mode presented here also suggests a way to biophysically characterize the interaction between PCNA and DNA. Because PCNA associates with DNA in a topological manner, structural and biophysical characterization

of this interface has been challenging due to the difficulty in producing a homogeneous population of PCNA:DNA complex for analysis. Similar hurdles exist for determining the structure of a ternary complex including PCNA and FEN-1 or DNA polymerase both bound to DNA. However, using the binding model presented here as a guide, it might be possible to covalently trap a complex of PCNA bound to DNA. The model of PCNA bound to DNA shows that some of the Lys residues located at the center of the PCNA ring (Lys14, Lys20, Lys80 and Lys217) interact close to the center of the minor groove. To trap a complex, it may be possible to use a strategy in which each of the target Lys residues are systematically mutated to Cys, and mixed with DNA containing G or T base with a commercially available alkanethiol modification (Midland Certified Reagent Company). These modifications would allow covalent trapping via formation of a disulfide bond (35). A similar strategy was used to trap HIV-RT bound to an RNA-DNA hybrid substrate (36), based on computational modeling of the interaction (37). This covalent trapping strategy would facilitate structural analysis of a PCNA:DNA complex by small angle X-ray scattering or X-ray crystallography. Thus, the results and concepts presented here provide a framework for a variety of experimental and computational approaches to test the functional implications of the asymmetric PCNA subunit interactions with DNA.

ACKNOWLEDGEMENTS

The authors thank Dr Tushar Jain for helpful discussions. Generous financial support was provided by the National Science Foundation and the National Institutes of Health. Additional support from the NSF Center for Theoretical Biological Physics (CTBP), National Biomedical Computational Resource (NBCR) and Accelrys, Inc. is also gratefully acknowledged. I.I. acknowledges support from the Burroughs Wellcome Fund in the form of a La Jolla Interfaces in Science interdisciplinary fellowship and J.A.T. support from CA081967 and CA92584. Computer resources were provided, in part, by the San Diego Supercomputer Center. Funding to pay the Open Access publication charges for this article was provided by the Howard Hughes Medical Institute.

Conflict of interest statement. None declared.

REFERENCES

- Krishna,T.S., Kong,X.P., Gary,S., Burgers,P.M. and Kuriyan,J. (1994) Crystal structure of the eukaryotic DNA polymerase processivity factor PCNA. *Cell*, **79**, 1233–1243.
- Kelman,Z. and O'Donnell,M. (1995) Structural and functional similarities of prokaryotic and eukaryotic DNA polymerase sliding clamps. *Nucleic Acids Res.*, **23**, 3613–3620.
- Gulbis,J.M., Kelman,Z., Hurwitz,J., O'Donnell,M. and Kuriyan,J. (1996) Structure of the C-terminal region of p21(WAF1/CIP1) complexed with human PCNA. *Cell*, **87**, 297–306.
- Moarefi,I., Jeruzalmi,D., Turner,J., O'Donnell,M. and Kuriyan,J. (2000) Crystal structure of the DNA polymerase processivity factor of T4 bacteriophage. *J. Mol. Biol.*, **296**, 1215–1223.
- Maga,G. and Hubscher,U. (2003) Proliferating cell nuclear antigen (PCNA): a dancer with many partners. *J. Cell. Sci.*, **116**, 3051–3060.
- Chapados,B.R., Hosfield,D.J., Han,S., Qiu,J., Yelent,B., Shen,B. and Tainer,J.A. (2004) Structural basis for FEN-1 substrate specificity and PCNA-mediated activation in DNA replication and repair. *Cell*, **116**, 39–50.
- Oku,T., Ikeda,S., Sasaki,H., Fukuda,K., Morioka,H., Ohtsuka,E., Yoshikawa,H. and Tsurimoto,T. (1998) Functional sites of human PCNA which interact with p21 (Cip1/Waf1), DNA polymerase δ and replication factor C. *Genes Cells*, **3**, 357–369.
- Shamoo,Y. and Steitz,T.A. (1999) Building a replisome from interacting pieces: sliding clamp complexed to a peptide from DNA polymerase and a polymerase editing complex. *Cell*, **99**, 155–166.
- Henneke,G., Friedrich-Heineken,E. and Hubscher,U. (2003) Flap endonuclease 1: a novel tumour suppresser protein. *Trends Biochem. Sci.*, **28**, 384–390.
- Hosfield,D.J., Mol,C.D., Shen,B. and Tainer,J.A. (1998) Structure of the DNA repair and replication endonuclease and exonuclease FEN-1: coupling DNA and PCNA binding to FEN-1 activity. *Cell*, **95**, 135–146.
- Sakurai,S., Kitano,K., Yamaguchi,H., Hamada,K., Okada,K., Fukuda,K., Uchida,M., Ohtsuka,E., Morioka,H. and Hakoshima,T. (2005) Structural basis for recruitment of human flap endonuclease 1 to PCNA. *EMBO J.*, **24**, 683–693.
- Bruning,J.B. and Shamoo,Y. (2004) Structural and thermodynamic analysis of human PCNA with peptides derived from DNA polymerase-delta p66 subunit and flap endonuclease-1. *Structure*, **12**, 2209–2219.
- Jorgensen,W.L., Chandrasekhar,J., Madura,J.D., Impey,R.W. and Klein,M.L. (1983) Comparison of simple potential functions for simulating liquid water. *J. Chem. Phys.*, **79**, 926–935.
- Essmann,U., Perera,L., Berkowitz,M.L., Darden,T., Lee,H. and Pedersen,L.G. (1995) A smooth particle mesh Ewald method. *J. Chem. Phys.*, **103**, 8577–8593.
- Ryckaert,J.P., Ciccotti,G. and Berendsen,H.J.C. (1977) Numerical integration of Cartesian equations of motion of a system with constraints—molecular dynamics of n-alkanes. *J. Comp. Phys.*, **23**, 327–341.
- Tuckerman,M., Berne,B.J. and Martyna,G.J. (1992) Reversible multiple time scale molecular dynamics. *J. Chem. Phys.*, **97**, 1990–2001.
- Kale,L., Skeel,R., Bhandarkar,M., Brunner,R., Gursoy,A., Krawetz,N., Phillips,J., Shinozaki,A., Varadarajan,K. and Schulten,K. (1999) NAMD2: Greater scalability for parallel molecular dynamics. *J. Comp. Phys.*, **151**, 283–312.
- Cornell,W.D., Cieplak,P., Bayly,C.I., Gould,I.R., Merz,K.M., Ferguson,D.M., Spellmeyer,D.C., Fox,T., Caldwell,J.W. and Kollman,P.A. (1995) A 2nd generation force-field for the simulation of proteins, nucleic acids, and organic molecules. *J. Am. Chem. Soc.*, **117**, 5179–5197.
- Saenger,W. (1984) *Principles of Nucleic Acid Structure*. Springer Verlag, NY.
- Ichiye,T. and Karplus,M. (1991) Collective motions in proteins—a covariance analysis of atomic fluctuations in molecular dynamics and normal mode simulations. *Proteins*, **11**, 205–217.
- Hunenberger,P.H., Mark,A.E. and van Gunsteren,W.F. (1995) Fluctuation and cross-correlation analysis of protein motions observed in nanosecond molecular dynamics simulations. *J. Mol. Biol.*, **252**, 492–503.
- Amadei,A., Linssen,A.B.M. and Berendsen,H.J.C. (1993) Essential dynamics of proteins. *Proteins*, **17**, 412–425.
- Lindahl,E., Hess,B. and van der Spoel,D. (2001) GROMACS 3.0: a package for molecular simulation and trajectory analysis. *J. Mol. Mod.*, **7**, 306–317.
- Mongan,J. (2004) Interactive essential dynamics. *J. Computer-Aided Mol. Design*, **18**, 433–436.
- Jonsson,Z.O. and Hubscher,U. (1998) Regulation of DNA replication and repair proteins through interaction with the front side of proliferating cell nuclear antigen. *EMBO J.*, **17**, 2412–2425.
- Johnson,A. and O'Donnell,M. (2005) Cellular DNA replicases: components and dynamics at the replication fork. *Annu. Rev. Biochem.*, **74**, 283–315.
- Kelman,Z. (1997) PCNA: structure, functions and interactions. *Oncogene*, **14**, 629–640.
- Li,X., Li,J., Harrington,J., Lieber,M.R. and Burgers,P.M. (1995) Lagging strand DNA synthesis at the eukaryotic replication fork involves binding and stimulation of FEN-1 by proliferating cell nuclear antigen. *J. Biol. Chem.*, **270**, 22109–22112.

29. Gomes, X.V. and Burgers, P.M. (2000) Two modes of FEN1 binding to PCNA regulated by DNA. *EMBO J.*, **19**, 3811–3821.
30. Lau, P.J., Flores-Rozas, H. and Kolodner, R.D. (2002) Isolation and characterization of new proliferating cell nuclear antigen (POL30) mutator mutants that are defective in DNA mismatch repair. *Mol. Cell. Biol.*, **22**, 6669–6680.
31. Fukuda, K., Morioka, H., Imajou, S., Ikeda, S., Ohtsuka, E. and Tsurimoto, T. (1995) Structure-function relationship of the eukaryotic DNA replication factor, proliferating cell nuclear antigen. *J. Biol. Chem.*, **270**, 22527–22534.
32. Kao, H.I., Henriksen, L.A., Liu, Y. and Bambara, R.A. (2002) Cleavage specificity of *Saccharomyces cerevisiae* flap endonuclease I suggests a double-flap structure as the cellular substrate. *J. Biol. Chem.*, **277**, 14379–14389.
33. Kaiser, M.W., Lyamicheva, N., Ma, W., Miller, C., Neri, B. and Lyamichev, V.I. (1999) A comparison of eubacterial and archaeal structure-specific 5'-exonucleases. *J. Biol. Chem.*, **274**, 21387–21394.
34. Pascal, J.M., Tsodikov, O.V., Hura, G.L., Song, W., Cotner, E.A., Classen, S., Tomkinson, A.E., Tainer, J.A. and Ellenberger, T. (2006) A flexible interface between DNA ligase and a heterotrimeric sliding clamp supports conformational switching and efficient ligation of DNA. *Mol. Cell*, **24**, 1–13.
35. Verdine, G.L. and Norman, D.P. (2003) Covalent trapping of protein-DNA complexes. *Annu. Rev. Biochem.*, **72**, 337–366.
36. Huang, H., Chopra, R., Verdine, G.L. and Harrison, S.C. (1998) Structure of a covalently trapped catalytic complex of HIV-1 reverse transcriptase: implications for drug resistance. *Science*, **282**, 1669–1675.
37. Bebenek, K., Beard, W.A., Darden, T.A., Li, L., Prasad, R., Luton, B.A., Gorenstein, D.G., Wilson, S.H. and Kunkel, T.A. (1997) A minor groove binding track in reverse transcriptase. *Nature Struct. Biol.*, **4**, 194–197.